Journal of Electronics and Electrical Engineering
https://ojs.wiserpub.com/index.php/JEEE/

Research Article

Hierarchical Control of AC/DC Hybrid Microgrid Based on Primary Model Predictive Optimization and Secondary Switching Control

Ziping Wang[1], Xiangkai Yu[1], Yinghao Shan[1,2*]

[1] College of Information Science and Technology, Donghua University, Shanghai, China
[2] Engineering Research Center of Digitized Textile and Apparel Technology, Ministry of Education, Shanghai, China
E-mail: shanyh@dhu.edu.cn

Received: 16 February 2024; **Revised:** 16 April 2024; **Accepted:** 28 April 2024

Abstract: The fluctuating characteristics of renewable energy generation in hybrid AC/DC microgrids, combined with timevarying loads, can result in high total harmonic distortion (THD) and distorted output voltage and current waveforms. To address these issues, a faster and more comprehensive primary and secondary hierarchical control method is required. In this paper, a faster model predictive optimization algorithm is introduced as a primary control method to predict operational states in advance, maintain a low THD state, and reduce the impact on power quality. Then, a secondary switching control is added to correct frequency and power allocation errors caused by primary control, recover microgrid voltage and frequency to their rated values, and ensure stable reactive power. Finally, simulation and comparison results prove the proposed method's effectiveness and applicability.

Keywords: hierarchical control, microgrid, model predictive optimization, switching control, power quality

1. Introduction

Microgrid is a small-scale power network that employs various distributed generations (DGs), storages, and protection devices to provide power. The system offers two ways of working: islanded and grid-connected. When operating in islanded, it acts as a stand-alone system that maintains its stability autonomously. Several inverters connected in parallel are used to convert DC to AC power. Moreover, the microgrid can operate in conjunction with the public grid, but it switches to islanded mode when functioning independently or when there's an issue with the external grid. However, microgrid systems are diverse and complex in their operation and power supply, making efficient control necessary for stability. To ensure this, two levels of control are involved: primary control for power distribution and conversion, and secondary control for power state restoration. The resulting two-layered control architecture is important for optimal performance of the system [1].

In current microgrids, droop control without interconnection lines is often used in islanded mode [2], while PQ control is usually used in grid-connected mode [3]. Droop control mimics the characteristics of synchronous generators by adjusting the output of inverters through voltage and frequency, thus controlling power distribution in the microgrid. As local loads increase, there may be a slight drop in voltage and frequency in the system due to the effect of droop control. To compensate for this deviation, secondary control of the system is required. Applying secondary control reduces the

DOI: https://doi.org/10.37256/jeee.3120244464

frequency and voltage amplitude deviation resulted from droop control, thus restoring them to their rated values and ensuring the power distribution capability of droop control simultaneously.

In primary control, after power droop control allocation, voltage and current dual-loop control is often required to generate PWM control signals to drive power conversion. Currently, there are studies that replace the aforementioned dual-loop control with equipment-level model predictive control (MPC) [4, 5]. For example, in [6] an improved MPC-based strategy is proposed to mitigate low-frequency oscillation from PV generation. The strategy analyzes both AC and DC sides of the VSC to improve performance in PV-based microgrids. In [7], controllers are designed with multipurpose MPC strategy use dynamic current and VSC voltage, making them suitable for grid-connected and island operation modes and transferrable between them. To avoid suboptimal performance with uncertainties from the conventional MPC for grid-forming inverters in microgrids, a new model-free predictive control is proposed in [8]. In [9], a new MPC for 3-phase bidirectional power inverters is presented in renewable-based microgrids, which applies sliding mode theory to attain effective dynamic response and minimize computational load. On the other hand, research on MPC in microgrids often focuses on system optimization. By measuring the internal disturbance signals within the microgrid, such as load variations, renewable energy fluctuations, battery status, network connection changes, etc., MPC can promptly adjust control strategies, enabling the microgrid system to more effectively respond to external changes and achieve greater stability and reliability in operation. For example, microgrids manage energy based on user preferences, weather, prices, and technical constraints using an MPC framework in [10, 11] that handles forecast errors and disturbances with perfect knowledge of microgrid state and renewable energy. The paper [12] presents the MPC framework, which utilizes the alternating direction method of multipliers to adaptively manage distributed energy resources and execute control actions at each time step. A new MPC strategy for optimal power flow in an AC microgrid is presented in [13]. It uses a simplified optimization problem based on a linear d-q voltagecurrent model and approximates the power flow linearly for a fast and reliable solution. In [14], a novel adaptive controller is proposed to mitigate the destructive effect of time-varying uncertain constant power loads (CPLs). A nonlinear disturbance observer is developed to estimate the instantaneous power of the CPLs. The estimated CPLs powers are then employed in a Takagi–Sugeno fuzzy-based MPC strategy. Experimental results show that the proposed adaptive controller is able to increase the stability margin and improve the transient response of the DC microgrid.

To put it simply, the use of MPC in microgrids focuses on controlling power conversion at the device level and optimizing at the system level. However, there is currently very little optimization of MPC for device-level power conversion control. Nevertheless, MPC has distinct advantages over ordinary linear methods as a multivariable control and optimization strategy, including intuitive concepts, rapid dynamic response, and flexible handling of multiple control objectives and constraints [15, 16, 17]. Therefore, at the primary control level, current research shows a need for optimizing the linear power conversion control method through the use of MPC.

In secondary control, there are several common methods, including centralized, distributed, and discrete methods [18]. Typically, voltage and frequency information at the point of common connection (PCC) is collected in real-time to eliminate steady-state errors through controllers with integral functions, allowing the system to recover its rated value. For this study, a centralized signal sampling mechanism is used, followed by a discrete local control strategy, which includes designing secondary controllers within each DG.

Overall, in primary control, power electronic devices such as inverters and rectifiers are typically utilized to convert the direct current output of renewable energy sources into alternating current. These power electronic devices often exhibit nonlinear characteristics, with switch operations introducing high-frequency harmonics. These nonlinear characteristics contribute to an increase in harmonic components within the system. Additionally, renewable energy systems may inject power into the microgrid at different frequencies and amplitudes under varying operating conditions. This uneven power injection results in fluctuations in the frequency and amplitude of voltage and current, further contributing to the increase in harmonic components, leading to an increase in THD values. To solve this problem, an MPC optimization method is introduced into the linear dual-loop control based on droop control strategy. This method leverages the responsive and dynamic performance of MPC to decrease the THD value of the system, ultimately improving the quality of electrical energy. Introduction of MPC optimization may lead to instability in the reactive power of the system. Thus, it is necessary to consider incorporating secondary control here. The secondary switching control can dynamically adjust control parameters and more flexibly handle external disturbances, thereby reducing the deviations resulted from droop control. This also

ensures a balanced reactive power system after grid connection. For this paper, a hybrid AC/DC microgrid will be utilized, as illustrated in Figure 1, as the research platform. This paper makes the following key contributions:

(1) To solve the problem of excessive THD during transient state of mode changes, the MPC optimization is introduced. Compared with traditional control methods, MPC has advantages such as faster response and lower THD, which not only increases the system stability, but also reduces the harm of harmonics to the PCC.

(2) To solve the problem that reactive power cannot be stable after microgrid is connected to the grid, secondary switching control is added to the controller. This reduces the amplitude deviations generated from droop control, while ensuring the quality of system output voltage and the balance of reactive power.

The following content of this paper is organized as such: the proposed MPC optimization method is described in Section 2 for primary level; Section 3 presents the proposed method for secondary switching control; Section 4 conducts simulation verification and result analysis discussion; and finally, the conclusion is provided in Section 5.

2. Primary MPC optimization

Droop control in the primary control level is responsible for managing the inverter in a distributed power system, allowing for newly connected loads to be shared. However, the process can create harmonics that have a negative impact on power quality and the lifespan of components. In order to address this situation, it is necessary to decrease the level of harmonics. One way to achieve this is by introducing an MPC based on the droop control strategy, which can enhance microgrid stability and practicality.

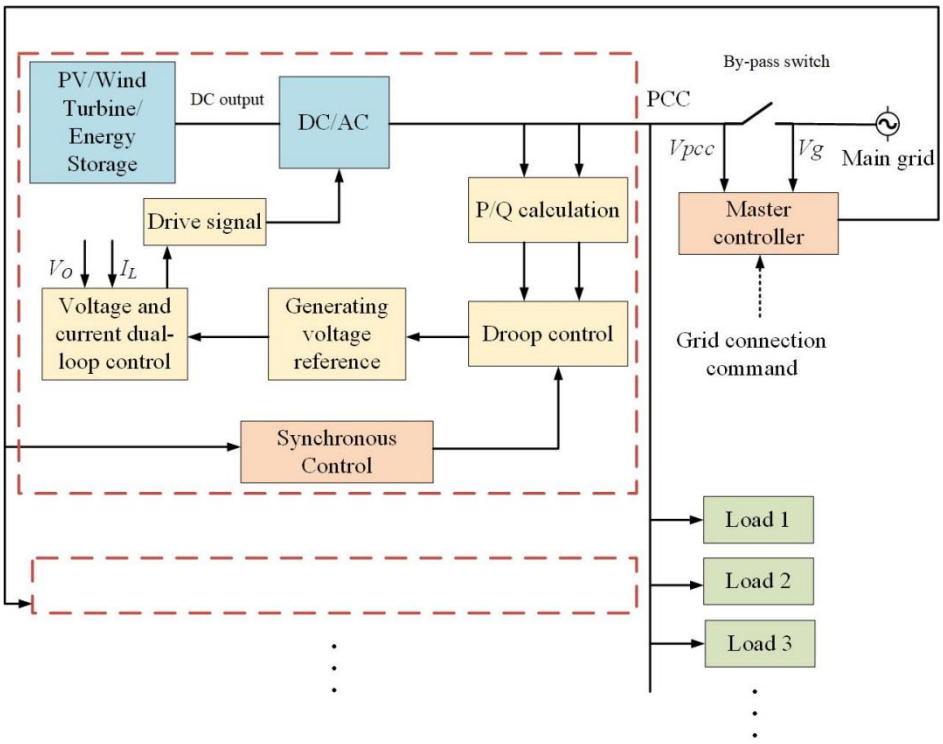

Figure 1. Topology of the hybrid microgrid.

2.1 *Primary droop control*

The working principle of droop control involves detecting the real-time output power of the inverter and using it to regulate its output voltage. The Figure 2 shows the simplified structure of two DG systems in parallel within a microgrid, with the power converter as the focus. In the figure, $U_1 \angle\phi_1$ and $U_2 \angle\phi_2$ represent the no-load output voltages, where ϕ_1 and ϕ_2 denote the no-load output voltage phases. $E \angle 0$ is the parallel bus voltage. $Z_i \angle\theta_i = R_i + jX_i$ is the sum of the output impedance and line impedance of DG_i (i = 1, 2). Where $\theta_i = \arctan(R_i/X_i)$ is the impedance angle. Z_L is the common load impedance. I_0 is the common bus current, while I_{L1} and I_{L2} denote the output currents of DG_i (i = 1, 2). The output powers P and Q of DG_i can be calculated using the following formula.

$$P_i = \frac{1}{|Z_i|}\left[\left(EU_i\cos\varphi_i - E^2\right)\cos\theta_i + EU_i\sin\varphi_i\sin\theta_i\right] \tag{1}$$

$$Q_i = \frac{1}{|Z_i|}\left[\left(EU_i\cos\varphi_i - E^2\right)\sin\theta_i - EU_i\sin\varphi_i\cos\theta_i\right] \tag{2}$$

where $|Z_i|$ is the impedance magnitude corresponding to DG_i.

$$|Z_i| = \sqrt{R_i^2 + X_i^2} \tag{3}$$

If $Z_i \angle\theta_i$ is inductive, the droop method results in the following relationship.

$$\begin{cases} f = f_n - m(P - P_n) \\ U = U_n - n(Q - Q_n) \end{cases} \tag{4}$$

where f_n, U_n, P_n, and Q_n represent the reference values for frequency, voltage, active and reactive power respectively. The corresponding droop coefficients are denoted by m and n.

For ease of calculation, in practical applications, the instantaneous power output of DGs for the power control module is:

$$\begin{cases} P = u_d i_d + u_q i_q \\ Q = u_q i_d - u_d i_q \end{cases} \tag{5}$$

where u_d and u_q refer to the voltage on the grid side, while i_d and i_q are the output current.

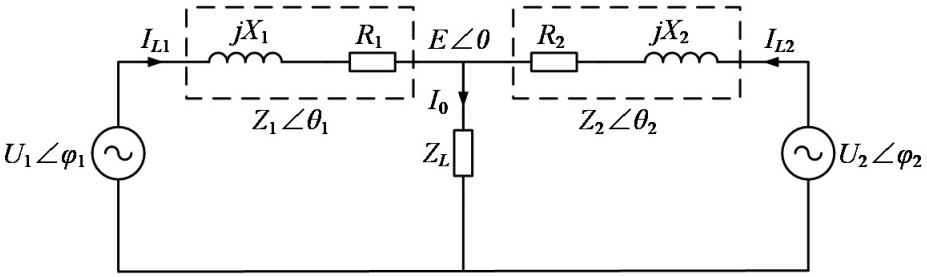

Figure 2. Simplified structure of two DGs in parallel.

2.2 *MPC optimization*

As mentioned earlier, MPC can be used to optimize primary control to improve power quality. MPC is a control strategy that aims to optimize the predicted future behavior of a system while adhering to specific constraints, and determines the ideal control sequence at each step of control [19, 20]. Once the first element of the control solution has been calculated, the controller proceeds to the next predicted step window and solves the optimization problem iteratively. MPC relies on utilizing a system model to forecast the outcomes of a specified control strategy.

Figure 3 illustrates the complete architecture of MPC, including the MPC module, the state estimation value calculation and the work module. Upon receiving the reference value $r(k)$ and disturbance value $w(k)$, the Kalman filter estimates the output value $y(k)$ of the operation module and sends the state value to the MPC. The MPC then outputs the optimal solution $v(k)$. Figure 4 demonstrates the MPC prediction process, which can forecast the impact on future system behavior.

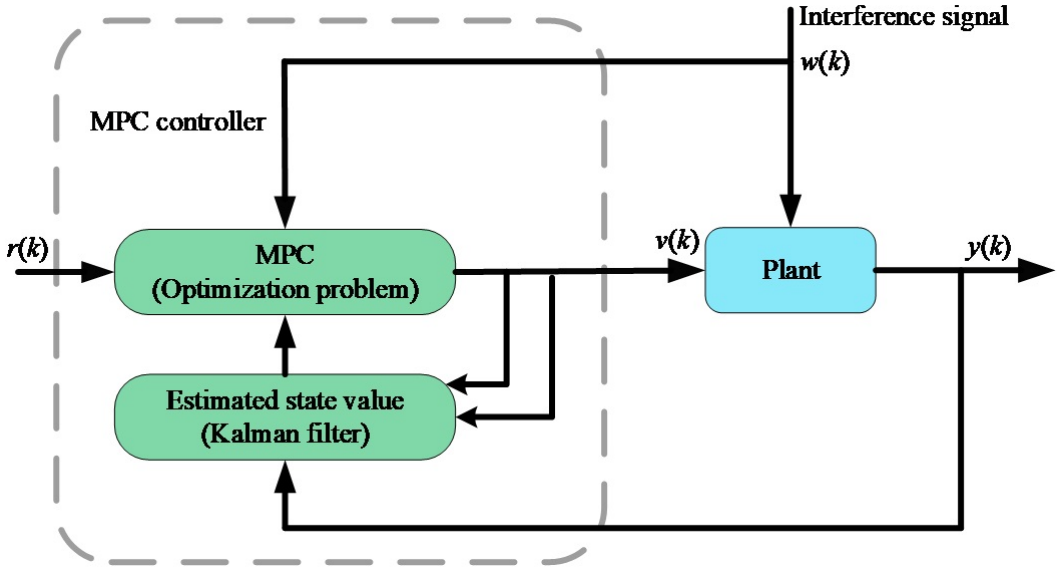

Figure 3. MPC architecture.

Linear and nonlinear models can be utilized to design an MPC controller for both single-input single-output and multiple-input multiple-output systems. In this case, the MPC's predictive system model is in its discrete-time statespace form with a specified sampling period T_{sp}, as shown in (6) and (7):

$$\begin{cases} x(k+1) = A_d x(k) + B_b u(k) \\ y(k) = C_d x(k) + D_d u(k) \end{cases} \tag{6}$$

$$u(k) = \begin{pmatrix} v(k) \\ w(k) \end{pmatrix} \tag{7}$$

where A, B, C, and D are matrices for the system, $x(k)$ represents the vector of state variables, $v(k)$ indicates the vector of control moves that have been calculated by MPC, $w(k)$ stands for the vector of measurement disturbances that affect the system, $y(k)$ represents measured system output vectors, and k indicates the sampling instant. The control objective, which is to track a given reference $r(k)$, is accomplished by solving an optimization problem of appropriate structure to obtain the optimal $v(k)$.

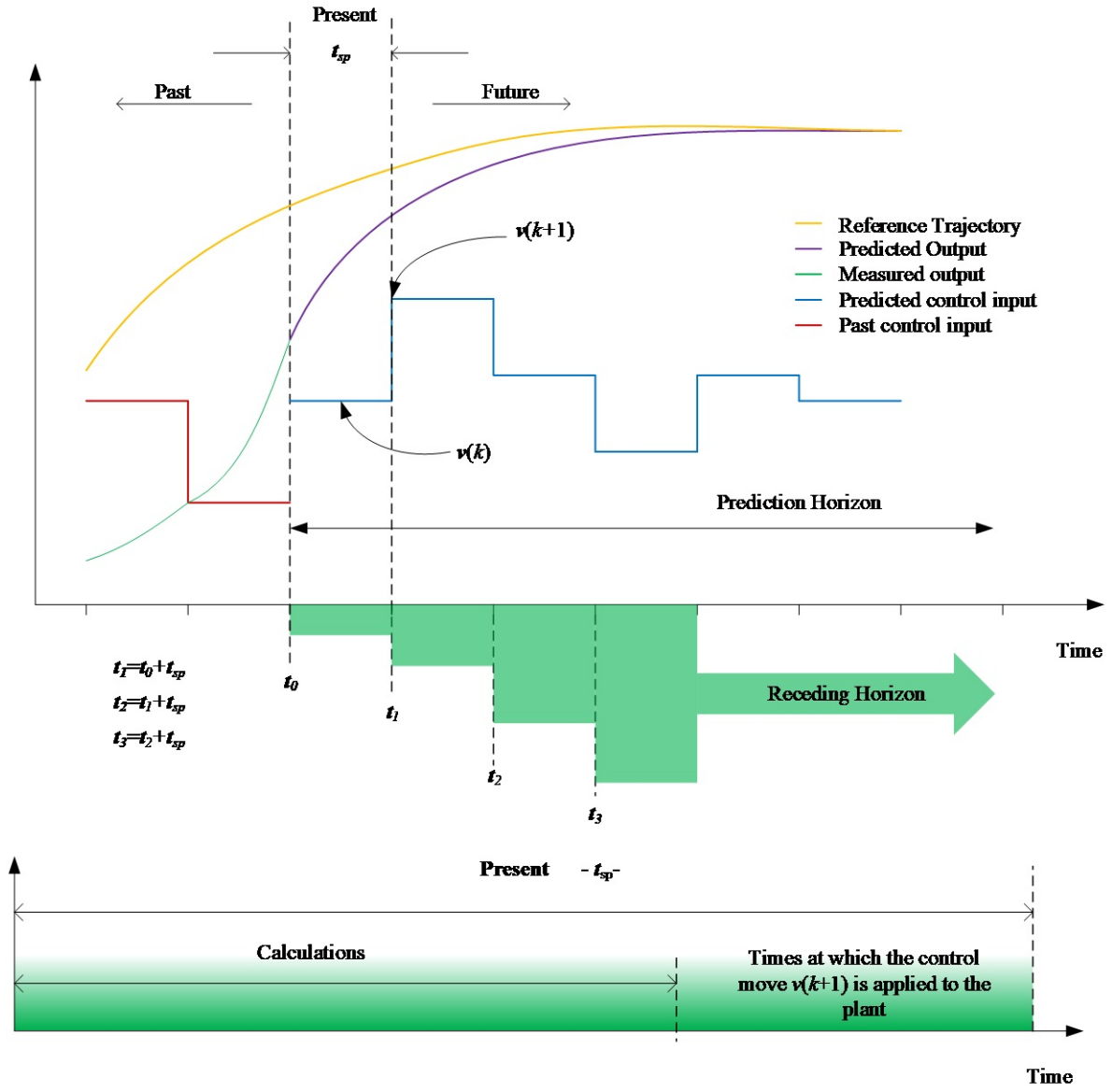

Figure 4. MPC evolution diagram example.

The MPC controller estimates the states using the Kalman filter in the state estimator, which can utilize sensor measurements and a system dynamic model to estimate the real-time values of each state variable in the microgrid, including the state and parameters of the system. These state estimates can be used as inputs to the MPC controller to adjust the control strategy in real time. Meanwhile, during each control interval, MPC solves an optimization problem, which is in the form of a quadratic programming problem, to determine the manipulated variables utilized as module inputs while satisfying the constraints until the next interval. In this optimization problem, it also exists a cost function, which must be minimized, as demonstrated in (8):

$$J(z_k) = J_y(z_k) + J_u(z_k) + J_{\Delta u}(z_k) + J_\varepsilon(z_k) \tag{8}$$

Each part in the above formula has a specific meaning. $J_y(z_k)$ is the target value for tracking y with reference to r, chosen to be zero across the entire prediction range. $J_u(z_k)$ tracks manipulated variables to maintain the controller's output

at target values. $J_{\Delta u}(z_k)$ suppresses changes in manipulated variables and controls deviations by comparing previous and current control commands. The main role of $J_{\varepsilon}(z_k)$ is to detect situations that do not conform to the constraint conditions.

The cost function formula written in quadratic form is commonly denoted as:

$$J = \sum_{l=1}^{n} \sum_{m=1}^{p} \left[\frac{w_{m,l}}{s_l} \{ r_l(k+m/k) - y_l(k+m/k) \} \right]^2 \tag{9}$$

Based on (9), the parts of (8) are written in quadratic form as follows:

$$J_y(z_k) = \sum_{l=1}^{n_y} \sum_{m=1}^{p} \left[\frac{w_{m,l}^{y}}{s_l^{y}} \{ r_l(k+m/k) - y_l(k+m/k) \} \right]^2 \tag{10}$$

$$J_u(z_k) = \sum_{l=1}^{n_u} \sum_{m=1}^{p-1} \left[\frac{w_{m,j}^{u}}{s_l^{u}} \{ u_l(k+m/k) - u_l(k+m-1/k) \} \right]^2 \tag{11}$$

$$J_{\Delta u}(z_k) = \sum_{l=1}^{n_u} \sum_{m=1}^{p-1} \left[\frac{w_{m,j}^{\Delta u}}{s_l^{u}} \{ u_l(k+m/k) - u_l(k+m-1/k) \} \right]^2 \tag{12}$$

$$J_{\varepsilon}(z_k) = \rho_{\varepsilon} \varepsilon_k^2 \tag{13}$$

Among them, k, p, n_u, n_y, and ε are the current control time, prediction range, number of manipulated variables, number of measured outputs, and adjustable variables, respectively. z_k is the command signal in the optimization problem. w and ρ_{ε} are weight adjustments made to ensure the required robustness.

The optimization problem is converted from an MPC optimization problem solver to a general optimization problem form, as seen in (14).

$$\min_{x} (\frac{1}{2} x^T H x + f^T x) s.t. \beta x \geq b \tag{14}$$

where the solution vector is denoted as x, the Hessian matrix is represented as H, and both b and f are vectors. H, β, b, and f are calculated by the controller at the start of each control interval. It is required that H is a positive definite value to allow the optimization problem to converge. The KWIK algorithm is used to solve the optimization problem. Once the constraint condition is satisfied by x, the algorithm terminates, where x^* is the optimal solution.

2.3 *Implementation of primary MPC*

The optimization issue discussed in this paper is resolved with the help of the MPC module in MATLAB/Simulink. This module is designed to accept the current output signal measurement (*mo*) and reference signal (*ref*), and can also select the measured disturbance signal (*md*). The default KWIK solver is utilized to solve the quadratic programming problem and thus calculate the optimal control variable (*mv*).

During the optimization process, it is necessary to design the main parameters of the MPC module. "*mo*" is the measured output, specified as a vector signal, which is used to improve its state estimate by using the measured device output. If the controller uses the default state estimate, the measured device output must be connected to the "*mo*" input port. The "*ref*" module output is a reference value, which can be either a row vector or a matrix signal. For consistency, use the same reference value from time (k + 1) to time (k + p) for the entire prediction horizon, where k is the current time and p is the prediction range. The "*mv*" signal is the best option for controlling manipulated variables, and should be outputted as a column vector. If the solver successfully finds a local optimal solution (qp.status is positive), then "*mv*" will contain that solution.

The Q-U droop unit can integrate the MPC module to improve its performance. The compensated voltage amplitude, with the rated voltage amplitude as reference, is inputted into the MPC. The output from the MPC passes through the PI controller, and the adjusted output is fed back to the system voltage. The proportional adjustment component of the PI controller responds to the system's deviation in proportion. In the presence of a deviation, the proportional regulator

generates a corrective effect, which is determined by the set parameters. The integral adjustment part of the PI controller can eliminate steady-state errors and improve the error-free degree of the system.

The effectiveness of the integral action is influenced by the time constant. By placing the PI controller at the MPC output position, errors caused by MPC can be eliminated, and system stability can be increased. The Q-U droop unit with added MPC module is shown in Figure 5.

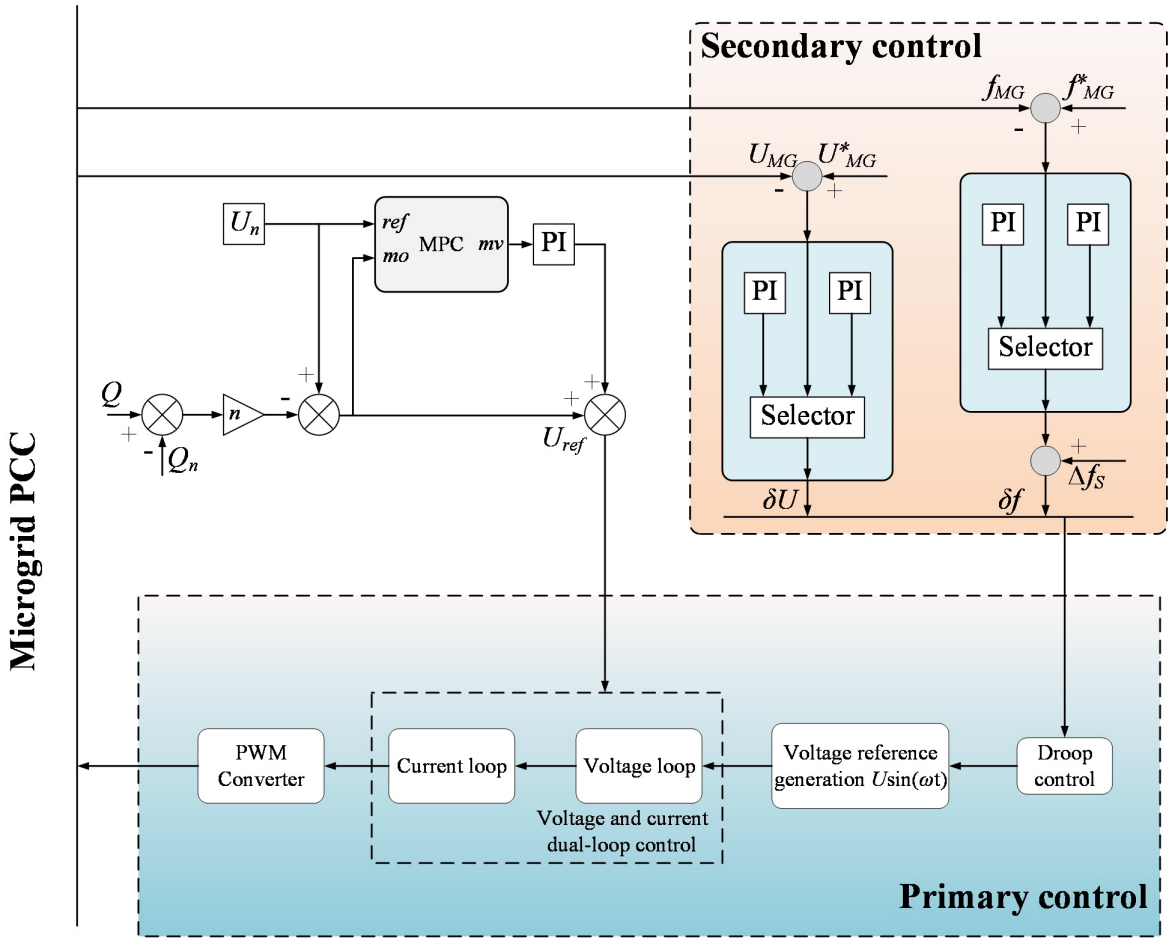

Figure 5. Primary and secondary controls of an AC microgrid.

3. Secondary switching control

3.1 *Secondary control*

A microgrid is a small power system that requires hierarchical control to function effectively. This control is usually divided into two layers: primary and secondary. The primary control layer manages the generation units, loads, and energy storage devices to maintain microgrid stability. The secondary control layer builds on the primary layer, further optimizing the overall operation of the system and enhancing the microgrid's reliability. By implementing hierarchical control, the microgrid can achieve intelligent control and operational optimization.

While droop control strategy has been successfully implemented to ensure smooth power allocation in microgrids, it has not resolved issues related to voltage and frequency errors. On the other hand, the introduction of MPC optimization has resulted in the inability to balance reactive power under droop control, which greatly impacts the stable operation

of the microgrid. To address this problem, introducing an external control loop called secondary control is necessary to restore the microgrid's internal frequency and voltage to their rated standard values.

Based on droop control, the microgrid secondary control is implemented through the following formula:

$$\begin{cases} f = f_n - m(P - P_n) + \delta f \\ U = U_n - n(Q - Q_n) + \delta U \end{cases} \tag{15}$$

where δf and δU are secondary control compensators. The compensation value will be added to the droop control formula, which will linearly enhance the droop curve, thereby maintaining the operating point under the original power distribution near the rated value. The value of the compensator is calculated specifically using the following formula:

$$\begin{cases} \delta f = k_{p\omega}(f^*_{MG} - f_{MG}) + k_{i\omega}\int (f^*_{MG} - f_{MG})dt + \Delta f_S \\ \delta U = k_{pE}(U^*_{MG} - U_{MG}) + k_{iE}\int (U^*_{MG} - U_{MG})dt \end{cases} \tag{16}$$

where $k_p\omega$, $k_i\omega$, k_{pE}, and k_{iE} are settings for the secondary control compensator, and Δf_S is the synchronization term, which is kept at zero when the microgrid is in island mode. Here δf and δU must be controlled within the allowable maximum frequency and voltage amplitude deviations.

3.2 *Switching control and implementation*

Microgrid switching control involves switching between two operation modes: islanded and grid-connected. This is crucial for maintaining a reliable power supply to important loads in microgrids. During grid-connected operation, the main power grid provides voltage and frequency support to the microgrid, and they exchange electrical energy at the common coupling point. If there is a fault in the power system, the microgrid can quickly and actively disconnect from the power system, smoothly switch to islanded operation, and independently distribute power from distributed energy sources to local loads. The smooth switching ensures that the voltage amplitude and frequency transient oscillation process during the switching process remains within the allowable fluctuation range.

In order to reduce frequency deviation and active power allocation errors in the system, secondary control employs PI compensators and compensations to synchronize and restore frequency and voltage. As previously mentioned, taking into account the characteristics of frequency/voltage droop control, secondary frequency/voltage control can be used. First, determine which stage the system is in and activate the corresponding control protocol. Then, under multi-stage coordination, provide compensation signals for the main control. Based on this, a secondary frequency control with two stages and a secondary voltage control with three stages are designed to strictly control the amplitude of frequency and voltage.

The design of the frequency switching controller is based on two stages: one where the frequency deviation value is large, and the other where it is small. The control protocol is as follows:

$$f_i(t) = f_n - m_i(Q_i(t) - Q_{ni}) + a_{1i}\delta_{1i}f_i(t) + a_{2i}\delta_{2i}f_i(t) \tag{17}$$

where a_{1i}, a_{2i} are the switches of each stage, whose values depend on the event generator; $\delta_{1i}f_i$, $\delta_{2i}f_i$ are the frequency compensations for stages one and two, respectively, which can be obtained from the following formulas.

$$\delta_{1i}f_i(t) = k_{1ifp}(f_n - f_i(t)) + k_{1ifi}\int (f_n - f_i(t))dt \tag{18}$$

$$\delta_{2i}f_i(t) = k_{2ifp}(f_n - f_i(t)) + k_{2ifi}\int (f_n - f_i(t))dt \tag{19}$$

where k_{1ifp}, k_{1ifi}, k_{2ifp} and k_{2ifi} are the PI control coefficients for the frequency first stage and second stage, respectively.

Event generators can detect the frequency range of received events, and then control the switch commands of different stages to trigger frequency control of the corresponding stages. Their settings are as follows:

$$\begin{cases} a_{1i} = 1, a_{2i} = 0; when f_i(t) \in (f_n, f_d] \\ a_{1i} = 0, a_{2i} = 1; when f_i(t) \in (f_d, f_{\max}] \end{cases} \tag{20}$$

where f_d is the preset triggering threshold, while f_{max} is the maximum allowable frequency value.

The purpose of secondary frequency control is to follow the control instructions of the event generator, improve the frequency produced by droop control, and create a compensating signal for primary frequency control. This process enables the restoration and stabilization of frequency.

Similar to frequency recovery, the two stages of larger and smaller nominal voltage deviation values can be considered for designing the secondary voltage switching controller, with the expression as follows:

$$U_i(t) = U_n + n_i(P_i(t) - P_{ni}) + b_{1i}\delta_{1i}U_i(t) + b_{2i}\delta_{2i}U_i(t) \tag{21}$$

where b_{1i} and b_{2i} are the switches of the secondary voltage in each stage; $\delta_{1i}U_i$ and $\delta_{2i}U_i$ are the voltage compensation signals in stages one and two, respectively, which can be calculated using the formulas below.

$$\delta_{1i}U_i(t) = k_{1iup}(U_n - U_i(t)) + k_{1iui}\int (U_n - U_i(t))dt \tag{22}$$

$$\delta_{2i}U_i(t) = k_{2iup}(U_n - U_i(t)) + k_{2iui}\int (U_n - U_i(t))dt \tag{23}$$

where k_{1iup}, k_{1iui}, k_{2iup}, and k_{2iui} are the PI control coefficients for the voltage first stage and second stage, respectively.

Similar to frequency control, we use the following formula (24) to configure switches in the event generator to coordinate the two stages:

$$\begin{cases} b_{1i} = 1, b_{2i} = 0; when U_i(t) \in (U_n, U_d] \\ b_{1i} = 0, b_{2i} = 1; when U_i(t) \in (U_d, U_{\max}] \end{cases} \tag{24}$$

where U_d is the preset triggering threshold, while U_{max} is the maximum allowable voltage value.

To reduce THD, MPC lowers the microgrid's reactive power. But this can cause instability. To fix this, a reactive power feedback step can be added. In grid-connected mode, the system will detect signals from the main grid and use secondary switching control to stabilize the reactive power and improve energy quality. The principle diagram for implementing secondary switching control is shown in Figure 5.

4. Simulation and analysis

Here, a hybrid AC/DC microgrid have been built, as illustrated in Figure 1, with the public AC bus serving as the connection point to the grid. The structure is mainly divided into 3 parts: wind turbine system, energy storage devices to ensure the voltage stability of the microgrid in island mode as well as rational distribution of power and droop control. Table 1. shows the system settings and control parameters. In order to simulate the stable switching of the microgrid from island mode to grid-connected mode and to show the speed of the system response within 2 s, it is in the island mode for $0 \leq t < 1$ s and enters the grid-connected mode for $t \geq 1$ s. When the microgrid receives the grid-connection command, the system detects the voltage and current information from the main grid, and once the grid synchronization requirements are met, the control strategy will switch from droop control to PQ control to complete the grid-connection process.

Table 1. System Setting and Control Parameter.

Description	Symbol and Value
System setting	f^* = 50 Hz, E^* = 380 V (p-p, rms), Electric power filter: L = 0.9 mH, C = 250 μF, Low-pass filter: 1/(0.015 s + 1), Power line: R = 0.05 Ω, L = 1.6 mH.
Primary control	M = −3/70,000 rad/W, n = 4/11,000 V/W, Outer-loop PI: 10 + 0.1/s, Inner-loop PI: 0.24 + 0.01/s.
Secondary switching control	k_{1fp}= 0.1, k_{1fi} = 12, k_{2fp}= 5, k_{2fi} = 12, k_{1up}= 0.8, k_{1ui} = 15, k_{2up} = 1.5, k_{2ui} = 15.

By calculating and comparing the THD values of the system under only PI control and under optimized control with the introduction of an MPC module, the output performance of the system can be seen intuitively. The THD values are compared in Figure 6. According to Figure 6, at t = 0.25 s, the microgrid system output voltage had not yet stabilized due to the startup of various units, resulting in many harmonics in the grid. However, the MPC method showed relatively low THD and better control strategy compared to the strategy without MPC. At t = 1 s, when the system switched from islanded to grid-connected mode, the THD under the PI control strategy is significantly higher than that under the MPC control strategy, indicating the effectiveness of MPC in improving power quality by suppressing harmonics.

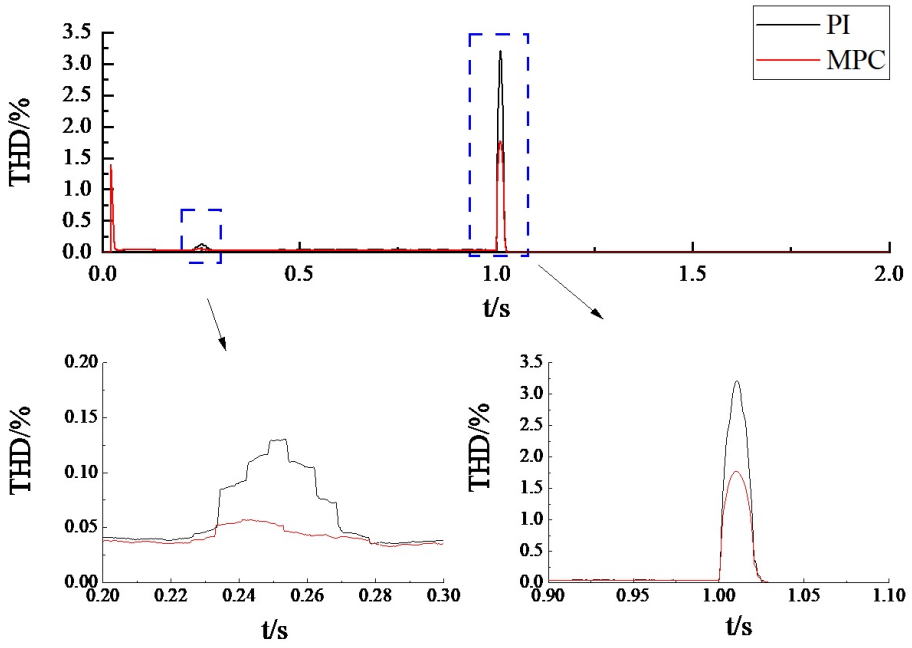

Figure 6. Comparison of THD with and without using MPC optimization method.

4.1 *Switching control in secondary control*

Switching control can seamlessly transition the microgrid from islanding operation mode to grid-connected operation mode, This is a crucial method to ensure continuous and reliable power supply for significant loads in the microgrid area. When the microgrid is in grid-connected mode, it exchanges power with the main grid at the public point of connection. Meanwhile, the frequency and voltage of the microgrid need to align with the main grid. When the main grid fails, the microgrid can swiftly transition from grid-connected mode to island mode, with distributed generators and batteries supplying power to local loads.

Subsequently, the microgrid's performance will be further enhanced by utilizing a secondary controller featuring switching control. To better showcase the microgrid's performance, a simulation will be performed for both grid-connected and islanded operation modes. The simulation will commence at $t = 0$, when the DC voltage output of the wind generator in the microgrid system has stabilized. From $t = 0$ to 0.5 s, the microgrid will operate in islanded mode, and at $t = 0.5$ s, it will be linked to the grid. At $t = 1.5$ s, it will disconnect from the grid and return to islanded mode. The local load will be set to 50 kW, and the parameters for this section are presented in Table 1. Performance parameters and output characteristics of the microgrid will be observed under these conditions.

The purpose of secondary control is to reduce the voltage and frequency errors resulted from the droop control strategy, and to bring the offset voltage and frequency back to the rated value. To compare the three-phase voltage values under the synergistic effect of secondary control and MPC and only PI control more intuitively, the peak voltage is selected for comparison. Therefore, the frequency and peak voltage waveforms are shown in Figures 7 and 8, respectively.

As presented in Figure 7, a stable frequency of 48.313 Hz is maintained by the microgrid under PI control in islanded mode, and a maximum frequency difference of 1.787 Hz is observed after grid connection. During the subsequent disconnection process, the frequency drops to a minimum of 48.300 Hz. The frequency difference Δf is greater than 0.1 Hz due to droop control between 0–0.5 s, and then secondary control is activated to restore the system frequency. Therefore, the maximum frequency difference after grid connection is only 0.541 Hz, and the system is re-stabilized at $t = 0.8$ s with the collaborative action of secondary switching control and MPC. During the subsequent disconnection process, the frequency drops to a minimum of 49.756 Hz, significantly improving the stability of the microgrid.

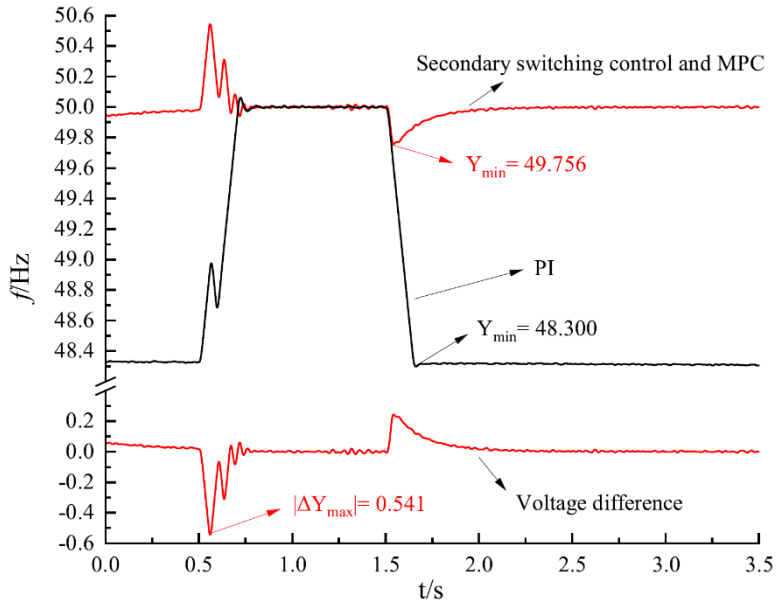

Figure 7. Frequency waveforms under the coordination of secondary switching control and MPC.

From Figure 8, it can be observed that a stable peak voltage output of 306 V in islanded mode is achieved by the microgrid with only PI control, and the peak voltage rises to the highest value of 436.1 V when it is connected to the grid, while the peak voltage output remains stable at 320 V after grid connection. When the secondary control is coordinated with MPC, the peak voltage output remains stable at 311 V, which is closer to the rated value than PI control, and the peak voltage drops to 297.5 V when connected to the grid. Throughout the entire process of switching from islanded mode to grid connection, the voltage is maintained at 311 V, and the maximum voltage difference of 12.5 V is achieved, which is much better than PI control.

As illustrated in Figure 9, prior to the incorporation of MPC and secondary switching control into the system, the THD value of the microgrid remained at an elevated level, significantly higher than the optimized THD value. During

the transitional process of switching from islanded to grid-connected mode, the THD value was temporarily elevated, potentially resulting in significant harm to both the microgrid and the main grid, ultimately posing a serious threat to the safety of electricity consumption for end-users.

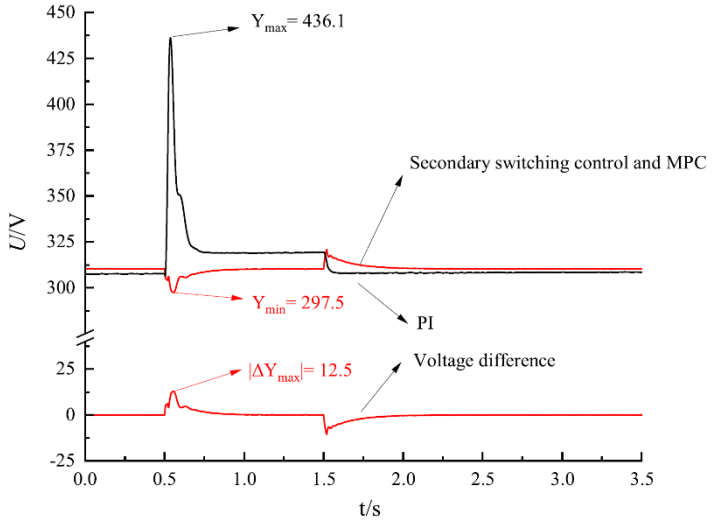

Figure 8. Voltage waveforms under the coordination of secondary switching control and MPC.

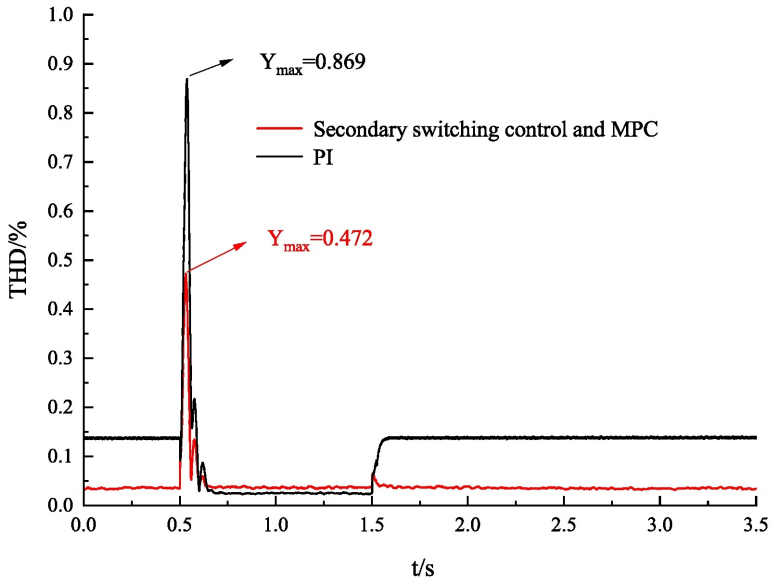

Figure 9. THD values under the coordination of secondary switching control and MPC.

From Figure 9, it can be observed that stable operation can be achieved in islanding mode with only PI control. However, the total harmonic distortion (THD) of the system is relatively high at approximately 0.14% on average. By contrast, when MPC and secondary switching control are employed, the THD is significantly reduced to an average of 0.03%. Consequently, optimized control methods greatly enhance the performance of the microgrid in islanding mode. Similarly, during the grid connection process, the highest THD of the system is reduced from 0.869% using only PI control to 0.472% with optimized control.

To maintain the stability and normal work of the microgrid's reactive power, it is necessary to check whether the reactive power is balanced. The focus is mainly on the reactive power status in islanded mode, as the reactive power of the

microgrid in grid-connected mode is determined by the main power grid under PQ control. Figure 10 shows the waveform of the reactive power during the entire operation of the microgrid. As can be seen in the figure, islanded operation mode was observed in the microgrid during the time intervals of 0–0.5 s and 1.5 s–3.5 s. Compared to the microgrid controlled only by MPC, the reactive power of the microgrid using secondary switching control coordinated with MPC control was converged and remained stable, resulting in an improvement in the microgrid stability.

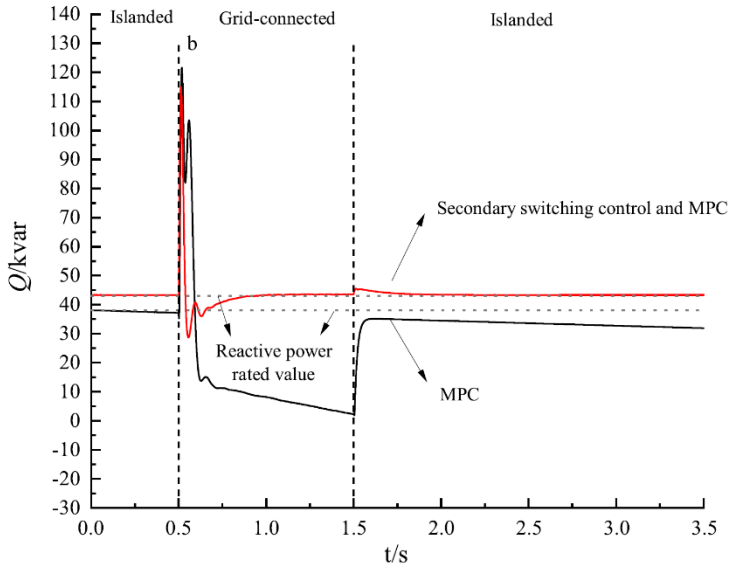

Figure 10. Reactive sharing under the coordination of secondary switching control and MPC.

5. Conclusions

This paper establishes a hierarchical control architecture with primary MPC optimization and secondary switching control. In comparison to microgrids that rely on traditional droop and power conversion control, this paper finds that the use of secondary switching control coordinated with MPC optimization yields greater stability. The output voltage of microgrid under islanded and grid-connected modes is improved, leading to an average output voltage of 99.6% of the rated value. The proposed control method in this paper reduces the peak reactive power by 10% during the microgrid transition from islanded to grid-connected mode, resulting in an improved transient performance of the system.

Acknowledgment

This work was supported in part by the Shanghai Sailing Program, China under Grant 21YF1400100, and in part by the Fundamental Research Funds for the Central Universities, China under Grant 2232021D-38.

Conflict of interest

There is no conflict of interest for this study.

References

[1] J. M. Guerrero, J. C. Vasquez, J. Matas, L. G. de Vicuna, and M. Castilla, "Hierarchical Control of Droop-Controlled AC and DC Microgrids—A General Approach Toward Standardization," *IEEE Trans. Ind. Electron.*, vol. 58, pp. 158–172, 2011, doi: 10.1109/tie.2010.2066534.

[2] U. B. Tayab, M. A. Bin Roslan, L. J. Hwai, and M. Kashif, "A review of droop control techniques for microgrid," *Renew. Sustain. Energy Rev.*, vol. 76, pp. 717–727, 2017, https://doi.org/10.1016/j.rser.2017.03.028.

[3] S. Adhikari and F. Li, "Coordinated V-f and P-Q Control of Solar Photovoltaic Generators With MPPT and Battery Storage in Microgrids," *IEEE Trans. Smart Grid*, vol. 5, pp. 1270–1281, 2014, https://doi.org/10.1109/tsg.2014.2301157.

[4] J. Hu, Y. Shan, J. M. Guerrero, A. Ioinovici, K. W. Chan, and J. Rodriguez, "Model predictive control of microgrids—An overview," *Renew. Sustain. Energy Rev.*, vol. 136, p. 110422, 2020, https://doi.org/10.1016/j.rser.2020.110422.

[5] Z. Zhang, Z. Zhang, O. Babayomi, O. Babayomi, T. Dragicevic, T. Dragicevic, R. Heydari, R. Heydari, C. Garcia, and C. Garcia, "Advances and opportunities in the model predictive control of microgrids: Part I-Primary layer," *Int. J. Electr. Power Energy Syst.*, vol. 134, 2022, https://doi.org/10.1016/j.ijepes.2021.107411.

[6] Z. Zhao, S. Gong, Q. Yang, J. Xie, X. Luo, J. Zhang, Q. Ni, and L. L. Lai, "An Improved FCS-MPC Strategy for Low-Frequency Oscillation Stabilization of PV-Based Microgrids," *IEEE Trans. Sustain. Energy*, vol. 14, pp. 2376–2390, 2023, https://doi.org/10.1109/tste.2023.3259204.

[7] M. Ghiasi, T. Niknam, M. Dehghani, H. R. Baghaee, Z. Wang, M. M. Ghanbarian, F. Blaabjerg, and T. Dragicevic, "Multipurpose FCS Model Predictive Control of VSC-Based Microgrids for Islanded and Grid-Connected Operation Modes," *IEEE Syst. J.*, vol. 17, pp. 2558–2569, 2022, https://doi.org/10.1109/jsyst.2022.3215437.

[8] R. Heydari, H. Young, F. Flores-Bahamonde, S. Vaez-Zadeh, C. Gonzalez-Castano, S. Sabzevari, and J. Rodriguez, "Model-Free Predictive Control of Grid-Forming Inverters With *LCL* Filters," *IEEE Trans. Power Electron.*, vol. 37, pp. 9200–9211, 2022, https://doi.org/10.1109/tpel.2022.3159730.

[9] L. Estrada, N. Vazquez, J. Vaquero, C. Hernandez, J. Arau, and H. Huerta, "Finite Control Set—Model Predictive Control Based On Sliding Mode For Bidirectional Power Inverter," *IEEE Trans. Energy Convers.*, vol. 36, pp. 2814–2824, 2021, https://doi.org/10.1109/tec.2021.3063601.

[10] A. Parisio, E. Rikos, and L. Glielmo, "A Model Predictive Control Approach to Microgrid Operation Optimization," *IEEE Trans. Control. Syst. Technol.*, vol. 22, pp. 1813–1827, 2014, https://doi.org/10.1109/tcst.2013.2295737.

[11] A. Parisio, C. Wiezorek, T. Kyntaja, J. Elo, K. Strunz, and K. H. Johansson, "Cooperative MPC-Based Energy Management for Networked Microgrids," *IEEE Trans. Smart Grid*, vol. 8, pp. 3066–3074, 2017, https://doi.org/10.1109/tsg.2017.2726941.

[12] T. Wang, D. O'Neill, and H. Kamath, "Dynamic Control and Optimization of Distributed Energy Resources in a Microgrid," *IEEE Trans. Smart Grid*, vol. 6, pp. 2884–2894, 2015, https://doi.org/10.1109/tsg.2015.2430286.

[13] T. Morstyn, B. Hredzak, R. P. Aguilera, and V. G. Agelidis, "Model Predictive Control for Distributed Microgrid Battery Energy Storage Systems," *IEEE Trans. Control. Syst. Technol.*, vol. 26, pp. 1107–1114, 2017, https://doi.org/10.1109/tcst.2017.2699159.

[14] N. Vafamand, S. Yousefizadeh, M. H. Khooban, J. D. Bendtsen, and T. Dragicevic, "Adaptive TS Fuzzy-Based MPC for DC Microgrids With Dynamic CPLs: Nonlinear Power Observer Approach," *IEEE Syst. J.*, vol. 13, pp. 3203–3210, 2018, https://doi.org/10.1109/jsyst.2018.2880135.

[15] S. Wen, W. Xiong, J. Cao, and J. Qiu, "MPC-based frequency control strategy with a dynamic energy interaction scheme for the grid-connected microgrid system," *J. Frankl. Inst.*, vol. 357, pp. 2736–2751, 2020, https://doi.org/10.1016/j.jfranklin.2019.12.001.

[16] Q. Yang, J. Zhou, X. Chen, and J. Wen, "Distributed MPC-Based Secondary Control for Energy Storage Systems in a DC Microgrid," *IEEE Trans. Power Syst.*, vol. 36, pp. 5633–5644, 2021, https://doi.org/10.1109/tpwrs.2021.3078852.

[17] F. Jiang and S. Cheng, "Additive-state-decomposition-based model predictive tracking control for PMSM servo system with multiple disturbances," *J. Frankl. Inst.*, vol. 360, pp. 9378–9398, 2023, https://doi.org/10.1016/j.jfranklin.2023.06.049.

[18] S. K. Sahoo, A. K. Sinha, and N. K. Kishore, "Control Techniques in AC, DC, and Hybrid AC–DC Microgrid: A Review," *IEEE J. Emerg. Sel. Top. Power Electron.*, vol. 6, pp. 738–759, 2017, https://doi.org/10.1109/jestpe.2017.2786588.

[19] F. Kamal and B. Chowdhury, "Model predictive control and optimization of networked microgrids," *Int. J. Electr. Power Energy Syst.*, vol. 138, 2022, https://doi.org/10.1016/j.ijepes.2021.107804.

[20] S. Negri, F. Giani, A. M. Pavan, A. Mellit, and E. Tironi, "MPC-based control for a stand-alone LVDC microgrid for rural electrification," *Sustain. Energy, Grids Netw.*, vol. 32, 2022, https://doi.org/10.1016/j.segan.2022.100777.